JOURNAL OF AIRCRAFT
Vol. 31, No. 2, March–April 1994

Determination of Tire-Wheel Interface Loads for Aircraft Wheels

S. Kandarpa,* B. F. Spencer Jr.,† and D. J. Kirkner‡
University of Notre Dame, Notre Dame, Indiana 46556
and
M. Champion§
Flight Dynamics Directorate, Wright-Patterson Air Force Base, Ohio 45433

A numerical tool is developed for determining the pressure distribution at the tire-wheel interface of an aircraft-wheel from experimentally obtained strains. The methodology employs an axisymmetric finite element model which is subjected to a general loading. The loading is represented as a double Fourier series, and the components are determined by a least squares fit using the experimentally determined strains. A finite element code based on linear elasticity for an isotropic material was developed to perform this analysis. Sample experiments are presented to illustrate the validity and the robustness of the algorithm. Finally, the limitations of this type of analysis are discussed and future directions are indicated.

Introduction

LANDING gear wheel failures have been responsible for a significant amount of aircraft damage.[1,2] Many such wheel failures have been catastrophic, resulting in a sudden loss of tire inflation pressure, and consequently, severe damage to primary aircraft structural systems. An FAA study by Durup and Brussat[1] showed that more than 30% of the over 5000 operational failures reported from 1970–1975 were due to wheel problems. This does not include wheels which were removed from service ahead of their expected service life because of cracks found during routine tire changes.

Design and analysis of an aircraft wheel requires that the applied loading be known or assumed.[3,4] Ground to tire loads are transmitted through the tire to the wheel at the tire-wheel interface (Fig. 1). Because tire behavior is nonlinear and difficult to accurately model, analytically determining the loads applied by the tire to the wheel is not an easy problem. Experiments have been conducted to directly measure the pressure distribution, but they have generally produced inaccurate results and are costly to perform.[5]

In this article, a new method is proposed for determining the loads transmitted from the tire to the wheel based on readily obtained strain measurements at various points on the wheel. The method will be shown to be accurate and inexpensive to employ. The results are intended for use in future studies of the durability and damage tolerance of aircraft wheels.

Problem Formulation

Consider the aircraft wheel depicted in Fig. 1. The geometry of the wheel and strain measurements at discrete points on the wheel surface are assumed to be available. From knowledge of the geometry and the boundary conditions of the wheel, an axially symmetric finite element model is developed which is subjected to a general loading. This model will be used to analytically back-calculate the load distribution at the tire-wheel interface (also known as the bead-seat region) from the experimentally measured strains.

Although the geometry of the wheel in general is not axially symmetric due to lightening holes, brake lugs, etc., the wheel can be reasonably approximated as an axially symmetric body because the input analysis data is obtained in regions removed from geometric irregularities. By using this geometric simplification, analysis can be carried out on a two-dimensional axisymmetric domain rather than the original three-dimensional body, thus greatly reducing the computational effort.

In the proposed problem where tire-wheel interface loads are to be computed, the loading is not only asymmetric but also varies along the surface of the body. Herein we use a cylindrical coordinate system r, θ, z (Fig. 2). The surface load is expressed as a function of θ and s where s, the surface

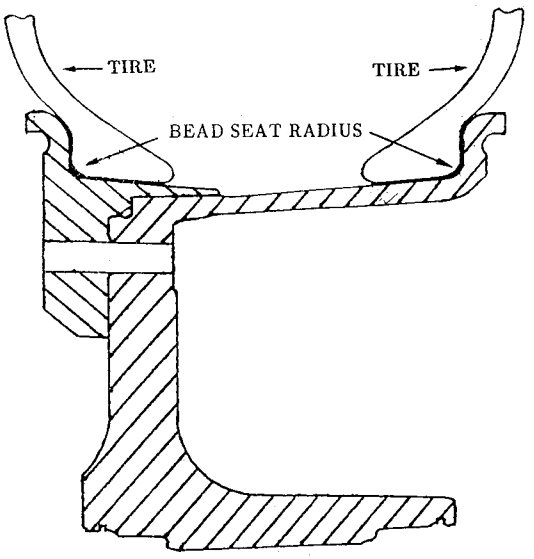

Fig. 1 Cross section of F-16 wheel and tire assembly showing the tire-wheel interface.

Presented as Paper 92-2482 at the AIAA 33rd Structural, Structural Dynamics, and Materials Conference, Dallas, TX, April 13–15, 1992; received May 4, 1992; revision received Dec. 28, 1992; accepted for publication Feb. 16, 1993.

*Graduate Assistant and Doctoral Candidate, Department of Civil Engineering and Geological Sciences.
†Associate Professor, Department of Civil Engineering and Geological Sciences. Member AIAA.
‡Associate Professor, Department of Civil Engineering and Geological Sciences.
§Mechanical Engineer, Landing Gear Systems Group.

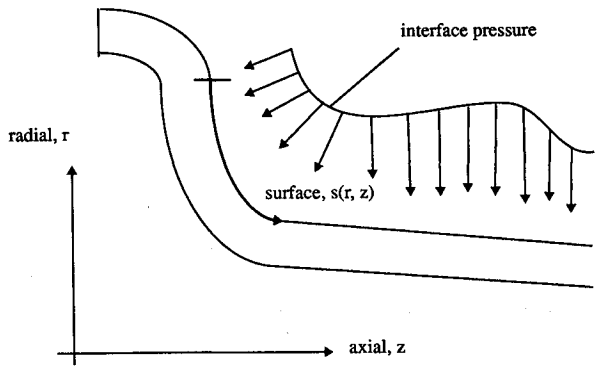

Fig. 2 Figure showing the r, z, and s coordinates, and interface pressure.

coordinate, is a function of r and z. The loading can be represented as a Fourier series in θ and s. The load $p(\theta, s)$ is thus given by

$$p(\theta, s) = \sum_n [p_{cn}(s)\cos(n\theta) + p_{sn}(s)\sin(n\theta)]$$

Furthermore, we may expand the coefficients $p_{cn}(s)$, $p_{sn}(s)$ in Fourier series over the interval of loading defined to be $0 < s < L$. Without loss of generality we use a Fourier cosine series. The final series representation is then given by

$$p(\theta, s) = \sum_m \sum_n \left[p_{cnm} \cos(n\theta)\cos\left(m\frac{\pi s}{L}\right) + p_{snm} \sin(n\theta)\cos\left(m\frac{\pi s}{L}\right)\right] \quad (1)$$

Consider a single loading component of unit amplitude

$$p_{cm}(\theta, s) = \cos(n\theta)\cos\left(m\frac{\pi s}{L}\right) \quad (2)$$

Let the strain response due to the above load be $\epsilon_{cnm}(r, \theta, z)$. All strains calculated in this article are based on a linear elastic and isotropic material response. The strain tensor at a point due to this loading can be decomposed as follows:

$$\epsilon_{cnm}(r, \theta, z) = \epsilon^c_{cnm}(r, z)\cos(n\theta) + \epsilon^s_{cnm}(r, z)\sin(n\theta) \quad (3)$$

where ϵ^c_{cnm} and ϵ^s_{cnm} are the cosine and sine amplitudes. If the load amplitude were p_{cnm} rather than unity, then the strain response would be $p_{cnm}\epsilon_{cnm}$. Similarly, the response due to a sine component loading

$$p_{sm}(\theta, s) = \sin(n\theta)\cos\left(m\frac{\pi s}{L}\right) \quad (4)$$

in the θ direction would be written as

$$\epsilon_{snm}(r, \theta, z) = \epsilon^c_{snm}(r, z)\cos(n\theta) + \epsilon^s_{snm}(r, z)\sin(n\theta) \quad (5)$$

The tensor coefficients, ϵ^c_{cnm} and ϵ^s_{snm}, in Eqs. (3) and (5) have the structure (see Appendix)

$$\epsilon = \begin{bmatrix} \epsilon_r & 0 & \gamma_{rz}/2 \\ 0 & \epsilon_\theta & 0 \\ \gamma_{rz}/2 & 0 & \epsilon_z \end{bmatrix} \quad (6)$$

whereas ϵ^s_{cnm} and ϵ^c_{snm} have the structure

$$\epsilon = \frac{1}{2}\begin{bmatrix} 0 & \gamma_{r\theta} & 0 \\ \gamma_{r\theta} & 0 & \gamma_{\theta z} \\ 0 & \gamma_{\theta z} & 0 \end{bmatrix} \quad (7)$$

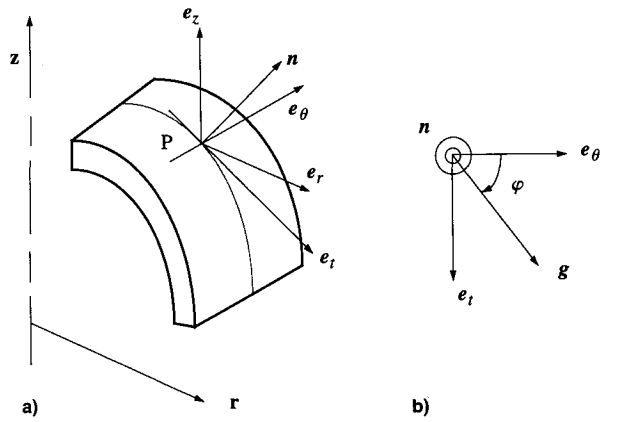

Fig. 3 Directions of strain vectors, e_z, e_o, and e_t with respect to: a) an axisymmetric body and b) vector g at which strains are computed.

The total response due to the loading as given in Eq. (1), by superposition, would then be

$$\epsilon(r, \theta, z) = \sum_n \sum_m (p_{cnm}\epsilon_{cnm} + p_{snm}\epsilon_{snm}) = \sum_n \sum_m \{p_{cnm}[\epsilon^c_{cnm}\cos(n\theta) + \epsilon^s_{cnm}\sin(n\theta)] + p_{snm}[\epsilon^c_{snm}\cos(n\theta) + \epsilon^s_{snm}\sin(n\theta)]\} \quad (8)$$

Since strain measurements will be taken on the surface of the body, an expression is needed for the direct strain on the surface in a specified direction. Referring to Fig. 3, it is required to find the strain on the surface of the body of revolution at a point with surface coordinate s and in a direction characterized by the unit vector g, defined with reference to Fig. 3 by

$$g = -m\sin(\varphi)e_r + \cos(\varphi)e_\theta + l\sin(\varphi)e_z \quad (9)$$

where m and l are direction cosines of the unit tangential vector e_t, and ϕ is the angle between the strain gauge placed on the surface of the body and the circumferential direction e_θ.

If $\epsilon(\theta, s)$ is the strain tensor of Eq. (9) evaluated at the point of interest on the surface, then the required direct strain is given by

$$\epsilon_g(\theta, s) = g^T\epsilon(\theta, s)g \quad (10)$$

Thus, we can write the series expansion for this direct strain as

$$\epsilon(\theta, s) = \sum_n \sum_m \{p_{cnm}[\epsilon^c_{cnm}\cos(n\theta) + \epsilon^s_{cnm}\sin(n\theta)] + p_{snm}[\epsilon^c_{snm}\cos(n\theta) + \epsilon^s_{snm}\sin(n\theta)]\} \quad (11)$$

where the subscript g is dropped for simplicity, but it should be kept in mind that all the strains in Eq. (11) are obtained by application of Eq. (10) to the component strain tensors of Eq. (8). Also note that Eq. (11) may be reordered as

$$\epsilon(\theta, s) = \sum_n \sum_m [(p_{cnm}\epsilon^c_{cnm} + p_{snm}\epsilon^c_{snm})\cos(n\theta) + (p_{cnm}\epsilon^s_{cnm} + p_{snm}\epsilon^s_{snm})\sin(n\theta)] \quad (12)$$

The direct strains are obtained experimentally at J locations and are denoted $\epsilon^*(s_j); j = 1, \ldots, J$ (in the direction defined by g as above). They may be decomposed into Fourier cosine and sine components and written as

$$\epsilon^*(s_j) = \sum_n [\epsilon^*_{cn}(s_j)\cos(n\theta) + \epsilon^*_{sn}(s_j)\sin(n\theta)] \quad (13)$$

Now comparing the cosine and sine terms of Eqs. (12) and (13) yields

$$\sum_{m=0}^{M} [p_{cnm}\epsilon^{c}_{cnm}(s_j) + p_{snm}\epsilon^{c}_{snm}(s_j)] = \epsilon^{*}_{cn}(s_j) \quad (14)$$

$$\sum_{m=0}^{M} [p_{cnm}\epsilon^{s}_{cnm}(s_j) + p_{snm}\epsilon^{s}_{snm}(s_j)] = \epsilon^{*}_{sn}(s_j) \quad (15)$$

where the series has been truncated after M terms.

Equations (14) and (15) can be concisely written in matrix notation as

$$\boldsymbol{E}_{nj}\boldsymbol{p}_n = \boldsymbol{\epsilon}^{*}_{nj} \quad (16)$$

where

$$\boldsymbol{E}_{nj} = \begin{bmatrix} \epsilon^{c}_{cn1}(s_j)\epsilon^{c}_{sn1}(s_j) & \cdots & \epsilon^{c}_{cnM}(s_j)\epsilon^{c}_{snM}(s_j) \\ \epsilon^{s}_{cn1}(s_j)\epsilon^{s}_{sn1}(s_j) & \cdots & \epsilon^{s}_{cnM}(s_j)\epsilon^{s}_{snM}(s_j) \end{bmatrix} \quad (17)$$

$$\boldsymbol{p}_n = [p_{cn1}p_{sn1} \cdots p_{cnM}p_{snM}]^T \quad (18)$$

$$\boldsymbol{\epsilon}^{*}_{nj} = \begin{bmatrix} \epsilon^{*}_{cn}(s_j) \\ \epsilon^{*}_{sn}(s_j) \end{bmatrix} \quad (19)$$

These equations are assembled together for all J experimental points resulting in

$$\boldsymbol{E}_n\boldsymbol{p}_n = \boldsymbol{\epsilon}^{*}_n \quad (20)$$

where

$$\boldsymbol{E}_n = [\boldsymbol{E}_{n1} \cdots \boldsymbol{E}_{nJ}]^T \qquad \boldsymbol{\epsilon}^{*}_n = [\boldsymbol{\epsilon}^{*}_{n1} \cdots \boldsymbol{\epsilon}^{*}_{nJ}]^T \quad (21)$$

Finally, premultiplying Eq. (20) by $\boldsymbol{E}^T_n$ results in the least squares equation

$$(\boldsymbol{E}^T_n\boldsymbol{E}_n)\boldsymbol{p}_n = \boldsymbol{E}^T_n\boldsymbol{\epsilon}^{*}_n \quad (22)$$

Solution of Eq. (22) yields the amplitudes of the Fourier components $\boldsymbol{p}_n$. This process is repeated for all $n = 0, \ldots, N$ in the θ direction. The amplitudes $\boldsymbol{p}_n$ are substituted into Eq. (1) and the load distribution on the contact surface is produced.

Sample Analysis and Results

The computer code ANTWIL (analysis of tire-wheel interface loads) was developed to integrate the algorithm described above with a finite element code for axially symmetric stress analysis with isoparametric four-node and eight-node elements. The results of several sample problems will be presented. These are presented to 1) demonstrate the validity and robustness of the algorithm, and 2) to find the rate of convergence required to reach an exact solution and thereby gain some understanding regarding the accuracy of results. Furthermore, these sample runs helped determine the minimum set of experimental data points required to perform a successful analysis.

The sample experiments were conducted in a three-step sequence. First, a known load is applied on the surface of the wheel (around the bead-seat region). By performing a finite element analysis, strain readings are obtained at J locations on the surface. Usually the strains were computed at the same locations as the experimental strains gauges and for this reason are called the experimental strains. These strains are stored in a vector of length $2J$, $\boldsymbol{\epsilon}^{*}_n$, where n corresponds to the harmonic number in the circumferential direction. It should be noted that in an actual analysis the first step is done experimentally. Next, the same analytical model is subjected to M unit harmonic loads in the s direction, for a specific n, and strains are determined at the same locations as the experimental strains. These analytical strains are then stored in a matrix $\boldsymbol{E}_n$ of dimension $2J \times M$ where each column of length $2J$ corresponds to the strains due to the mth Fourier load. Finally the Fourier amplitudes $\boldsymbol{p}_n$ are obtained by solution of the least squares Eq. (22). These amplitudes are substituted into Eq. (1), and the back-calculated load is obtained and then compared with the applied load for convergence and accuracy. Details of these sample experiments are given in the following sections.

Finite Element Mesh

The finite element mesh (Fig. 4) used here is from Lawler et al.[3] The mesh has 132 eight-noded isoparametric elements and 517 nodes. The mesh is highly refined near the bead-seat region where accurate knowledge of the strains is required for the load recovery algorithm. For demonstration purposes, loading on the inboard half of the wheel only was considered for the analysis.

Wheel Subjected to a Quadratic Load

A quadratic load as shown in Fig. 5 was applied on the bead-seat region of the wheel. This load can be represented as $p = as^2 + bs + c$, where s is the surface coordinate and p is the contact pressure or load. The analysis described above was performed and the applied load was recovered.

In the first numerical experiment, five strain readings ($J = 5$) were used. The locations of these readings are shown in Fig. 6. These strains were computed in the direction of $\boldsymbol{e}_t$ (Fig. 3) and for $n = 0$. The recovered load obtained from this

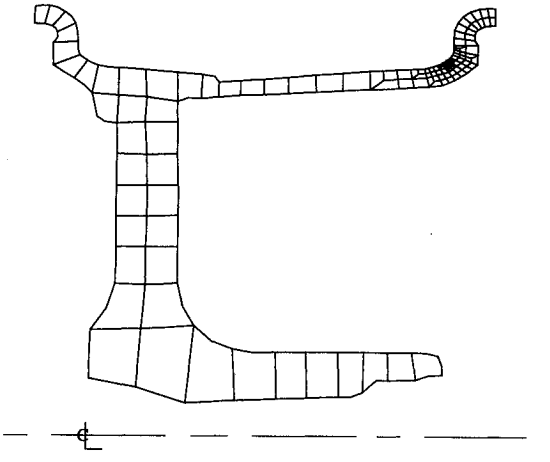

Fig. 4 Finite element mesh.[3]

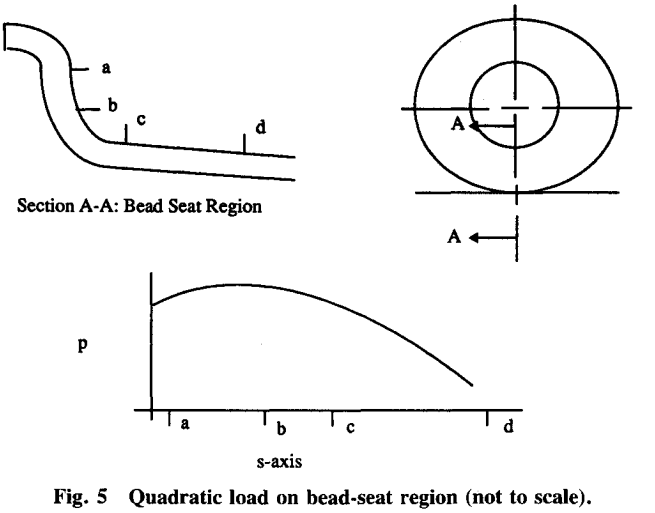

Fig. 5 Quadratic load on bead-seat region (not to scale).

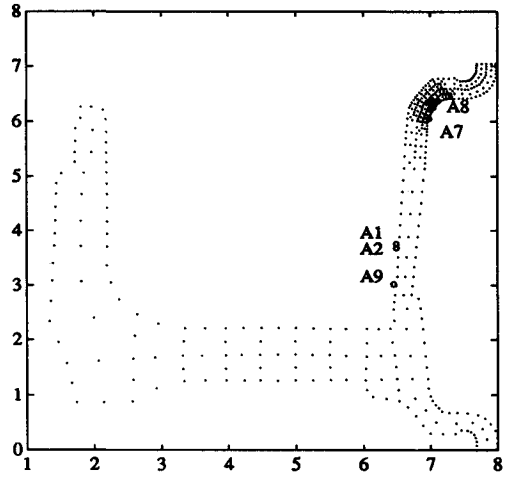

Fig. 6 Locations of strain readings.

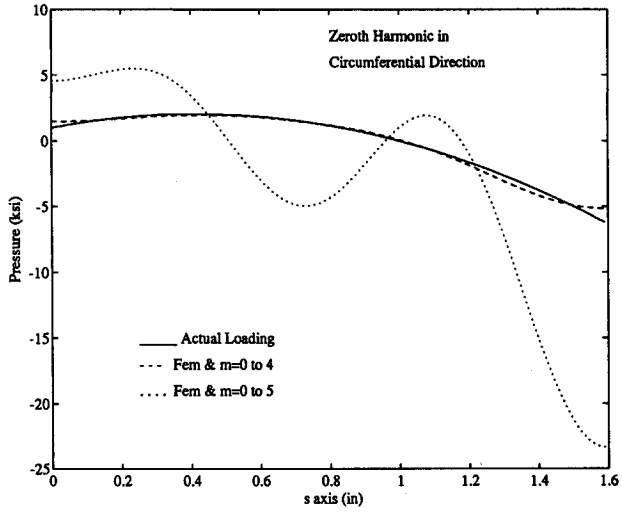

Fig. 7 Results of ANTWIL for five strain readings.

analysis was compared with the applied quadratic load and is shown in Fig. 7. For five harmonic terms (m = 0–4), the quadratic function is reproduced accurately, though convergence is not complete. It should be noted that (for an overdetermined case) the maximum number of harmonics that can be taken to represent a function equals the number of experimental strain locations (J). If more than J harmonics are taken then there are fewer equations than unknowns leading to an underdetermined system of equations. For this experiment the maximum number of harmonics was five; m = 0–4 and J = 5. As a result, when the number of harmonic terms in the series was increased to six, m = 0–5, singularities were found in the inverse of $\boldsymbol{E}_n^T\boldsymbol{E}_n$. The results are shown in Fig. 7.

In the next run the number of strain readings was increased to 10 (i.e., J = 10). The analysis was performed for m = 0–8 and m = 0–9. The results (Fig. 8) show convergence and are closer to the actual load. Therefore, it is seen that an increase in the number of strain readings increases accuracy of the results.

Simulated Load on the Wheel

In this numerical experiment, a load (Fig. 9) much more complicated than in the first example was applied on the wheel at the bead-seat region, and the output of the analysis in terms of strains was computed at specified locations. To evaluate the accuracy of the analysis, the number of places at which strains were computed was gradually increased, starting with five strain readings (J = 5; as in Fig. 5; A1, A2, A7, A8, and A9). In this case strains in the direction of e_t were considered.

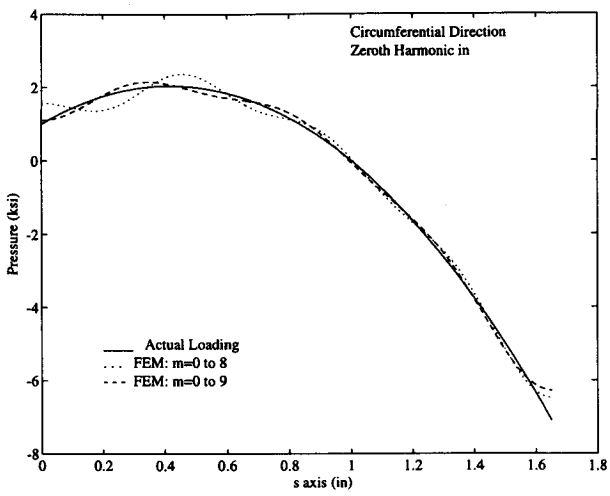

Fig. 8 Results of ANTWIL for 10 strain readings.

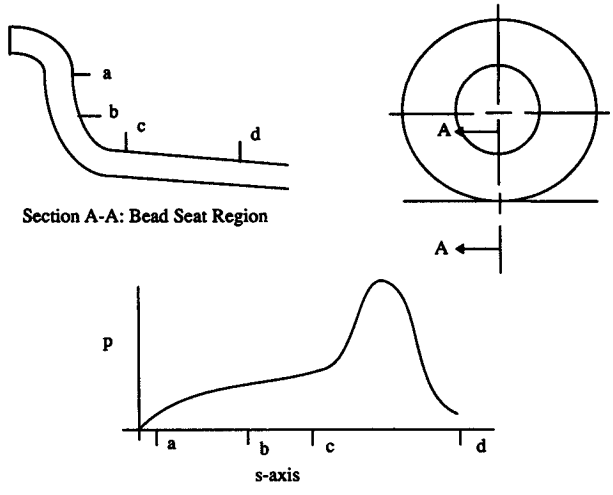

Fig. 9 Probable load on bead-seat region.

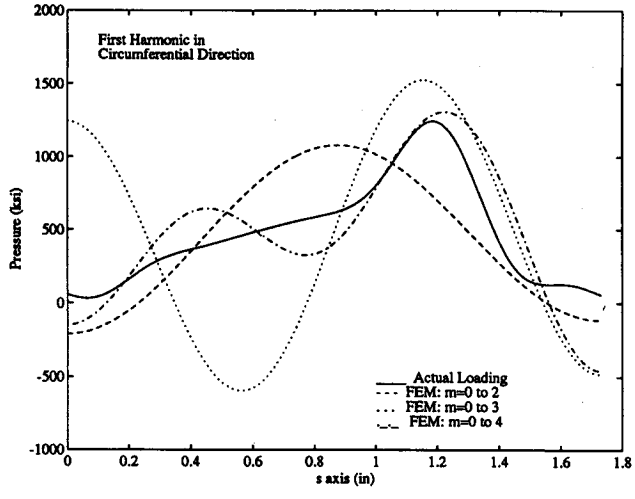

Fig. 10 Results for five strain readings.

The results obtained were oscillatory (Fig. 10) and were nowhere near the actual loading. Since the number of strain readings were inadequate to get accurate results, the number was increased to eight, i.e., three additional readings (C1–C3) were added to the original set of five (J = 8); again only tangential strains (in the e_t direction) were considered (Fig. 11). These additions were near the bead-seat region. The plots of these analyses are shown in Fig. 12. From this plot it can be seen that when the number of strain-output locations increased to eight, and for an analysis representing eight har-

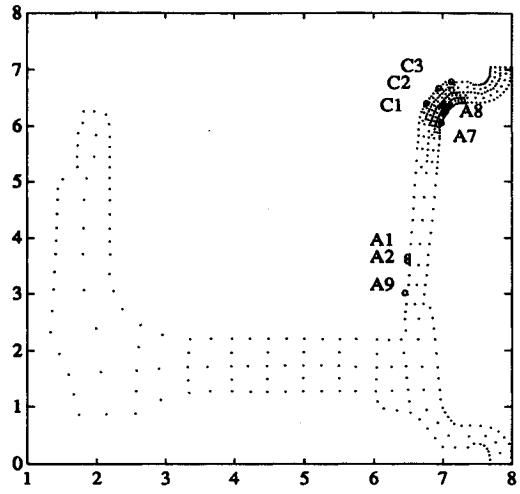

Fig. 11 Locations of eight strain readings.

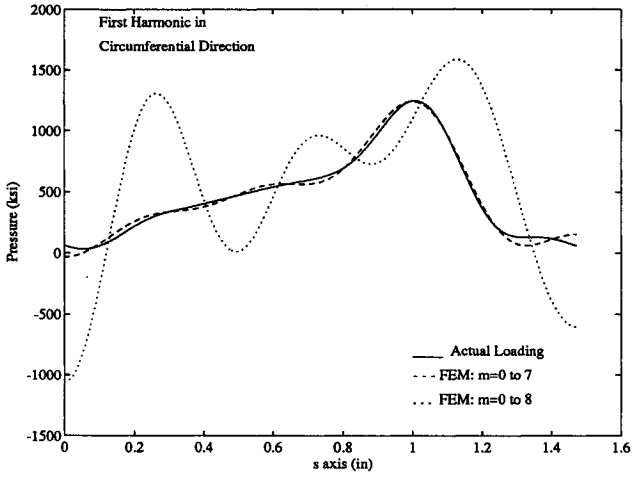

Fig. 12 Results for eight strain readings.

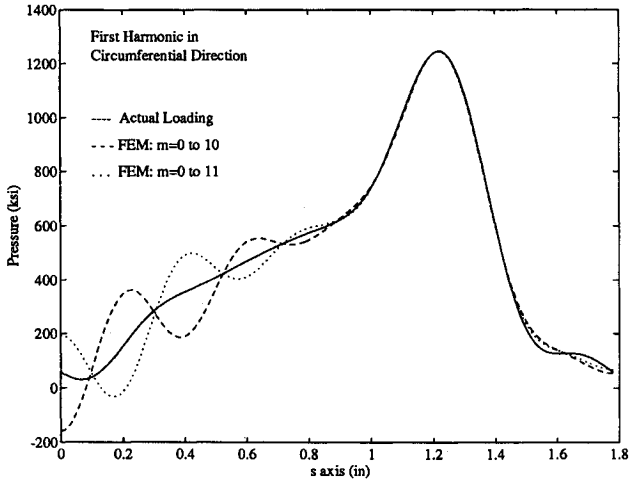

Fig. 13 Results for 12 strain readings.

monics (m = 0–7) the results matched well with the actual loading. This was considered a critical number of harmonics for this model as it was the minimum number of harmonics that represented the current loading function. When the analysis was performed for a higher number of harmonics (m = 0–8) for the same number of strain locations (J = 8), the results diverged as expected as this represented an underdetermined system of equations. Finally, two more runs were considered in which the total number of strain locations were increased to 12. As indicated in Fig. 13 the results of these runs showed convergence.

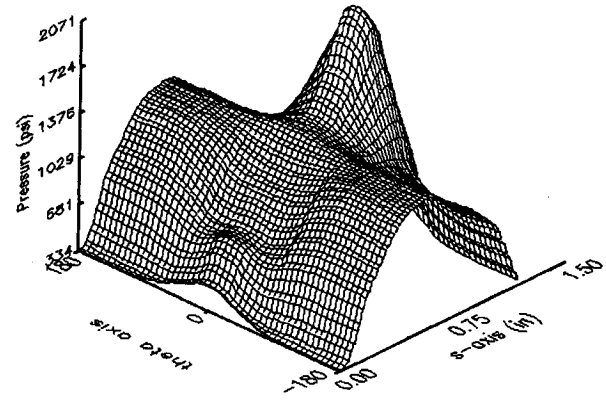

Fig. 14 Two-dimensional surface traction.

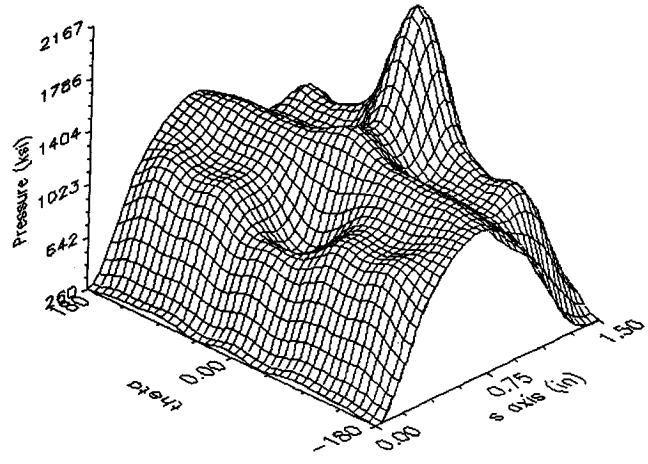

Fig. 15 Recovered traction for 11 strain readings.

The above analysis was carried out for the first harmonic in the circumferential direction. Similar results were also obtained for other harmonics in this direction.

Recovery of Two-Dimensional Surface Traction

This section will study the ability of the algorithm to recover a more realistic, two-dimensional surface load distribution. A sample load with θ and s variation was applied (Fig. 14). If taken only for θ = 0, this load would perfectly match the one-dimensional line load presented in Fig. 9. Upon applying this load, strains were obtained at the specified points on the surface. The idea herein was to use the knowledge of these strain data and the stated algorithm to regenerate the original loading. This is to simulate an actual test scenario where the specified strains would be obtained through experiments using strain gauges.

To apply the load, an analytical representation of the same is necessary. This was done using Fourier harmonic representation in two dimensions, θ and s. The Fourier representation was useful because the decomposed loads were directly used for performing the analysis. It should be noted that in an actual analysis the surface strains are decomposed in series of harmonics (m = 0, 1, . . . , M) in the circumferential direction. Individual analyses are carried out for each of these harmonics. Thus, by applying the decomposed loads in the circumferential direction for all harmonics, a set of strains are obtained for each harmonic which would be equivalent to the decomposed experimental strains. This is because the model chosen herein is linear.

The analytical representation of the loads is shown in Fig. 14. The analytical loads are then applied for each harmonic to obtain the individual strain data set at specific locations on the surface of the wheel. For the first run, a total of 11 strain

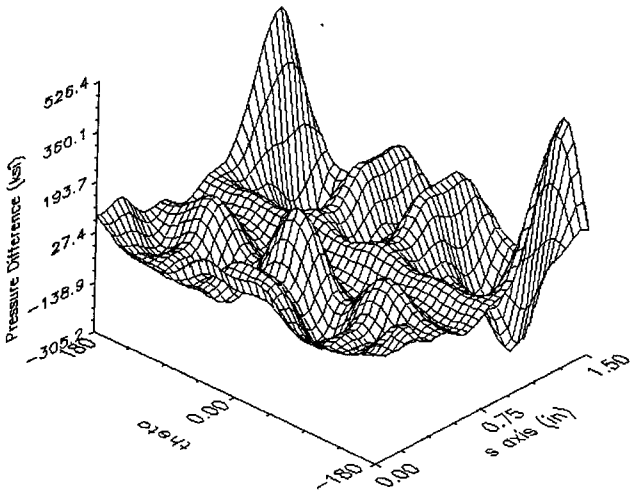

Fig. 16 Difference between the applied and the recovered traction.

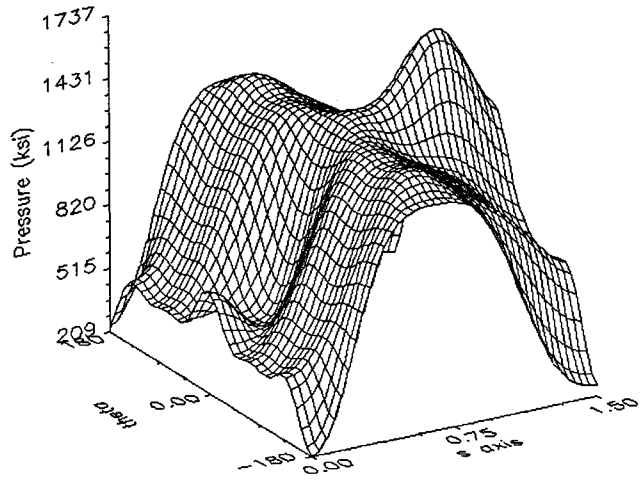

Fig. 17 Recovered load for eight strain readings.

readings $J = 11$ were chosen, of which eight were located around the bead-seat region and the remaining three on the flange. Using these representative strain data sets, analysis was carried out to recover the load that was applied to obtain the strain by using unit Fourier series in the s direction and then solving the least squares Eq. (22). The results for all individual harmonics were superposed to get the complete two-dimensional surface loading. This is shown in Fig. 15. Figure 16 is a plot of the difference between the applied and the recovered load (i.e., Figs. 14 and 15). It can be seen that at the point of maximum load the error is approximately 10%. In this analysis 11 representative strain readings were taken to perform the analysis. To see the effect of the number of strain readings on the convergence and accuracy of the final results various combinations of strain readings were taken. When the strain readings were increased to 14, the results obtained were almost similar to the one shown in Fig. 15, showing that the results have essentially converged. To check the lower limit on the number of strain readings, a total of seven strain readings were taken and the analysis was carried out. Out of these seven readings, five were located on the bead-seat region and the remaining two on the flange. The results of the analysis are shown in Fig. 17. It can be inferred from this particular figure that seven readings were insufficient to represent the original loading function as described in Fig. 14. Further analysis was carried out by adding an extra reading around the bead-seat region taking the total to eight readings. It was found that the results were much closer to the actual loading. Therefore, for this problem, eight readings were required to reproduce the original load distribution.

Experimental Data and Analysis

Experimental Data

Laboratory testing of the F-16 landing gear was performed at Wright Laboratory by the Landing Gear Development Facility. The idea behind this laboratory test was to obtain critical-strain readings which could be useful in understanding the behavior of the wheel under different types of loading. Strain gauges were located on an F-16 main wheel at critical-stress locations. A total of 26 gauges, 12 rosette gauges (36 gauge readings), and 14 single gauges for a total of 50 strain readings were used to obtain the strain data. Details of strain gauge locations and the procedure for the test are available.[6] A few strain gauges that were used in the finite element analysis are shown in Fig. 18.

The readings were taken at circumferential increments of less than one-half of one deg. To get an analytical representation of these strains, they were described by a series of harmonic functions by using Fourier analysis. This provided an accurate representation of the actual strain data. Only six cosine and sine terms were required ($n = 0-5$) to represent these functions. Series representation of the strain data was useful in decomposing the experimental strains in the circumferential direction. This was done by choosing the amplitudes of all valid strain gauges for a given harmonic in the θ direction and storing them in a vector ϵ_n^*; n represents the harmonic number. The results from the experimental strain data are reviewed in the following section.

Analysis of Experimental Data

While performing an analysis using the experimental data (this strain data pertains to a rolling test with a normal load of 16,820 lb, an inflation pressure of 298 psi, and zero yaw), it is important to note that the number of strain gauges available in the tubewell and bead-seat region is only five. The analysis was performed using these five strain gauges (A1, A2, A7, A8, and A9). As far as the pressure distribution at the bead-seat is concerned, strain gauges A3–A6, A15–A16, and B23 did not provide any relevant information and hence were not used in the analyses. This may be explained by Saint-Venant's principle. Strains located away from the loading area would provide little information regarding the tire-wheel interface pressure distribution.

Experimental strains, as mentioned, were represented effectively by six ($n = 0-5$) Fourier harmonics. It should be remembered that this representation is for the strains in the e_t direction. Each of these amplitudes for a given harmonic and for all five strains are combined to form a set of strains for that mode. Thus, there were six such strain sets and the results of all these sets when superposed would give the total-

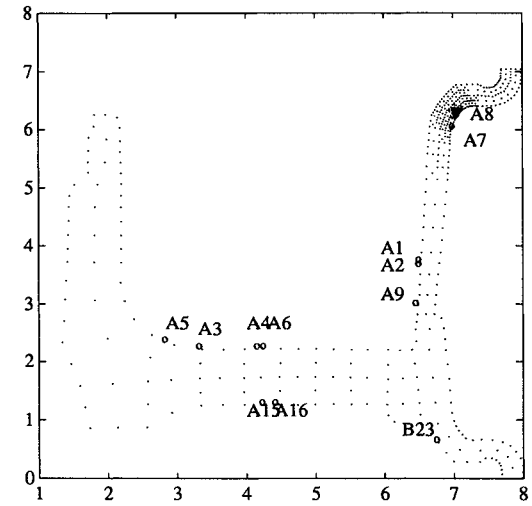

Fig. 18 Locations of experimental strain gauges that were modeled by finite element method.

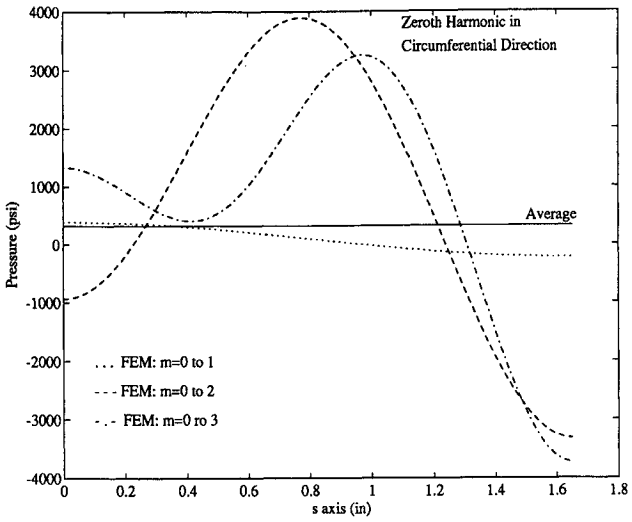

Fig. 19 Results of ANTWIL for zeroth harmonic in circumferential direction for the experimental data.

load effect in all three directions. The first analysis was performed on the set of strains which represented the zeroth harmonic ($n = 0$). The results for this harmonic are represented in Fig. 19. As the number of strain readings is only five ($J = 5$), the maximum number of terms that could be represented is also five ($m = 0$–4). The plots seemed to be inconclusive as far as predicting the shape of the actual load. This behavior was also expected from earlier sample analyses of a realistic load on the wheel. In fact it took at least eight terms to represent the entire loading function. For higher accuracy more terms were required (approximately 12). Similar results were obtained for the remaining five sets of strain readings. It should be noted that $m = 0$ actually represents the average of the overall loading for a given set of strains for that harmonic mode (in the circumferential direction).

Conclusions

The problem of back-calculating the normal loads at the tire-wheel interface given experimentally obtained strain data has been investigated. An algorithm using Fourier series representation of the loading and a least squares fit to experimental strain readings has been developed and seemed to be effective. This was demonstrated through several simple test cases. The study highlighted several important factors. First is the location of the strain gauges on the surface of the body. To capture the load characteristics around the bead seat region (or any region), it is imperative to have adequate strain readings in that region. This result is expected from Saint-Venant's principle and was shown to be correct when strains around the web region (A3–A6, A15–A16) were used for computation of the load distribution around the bead-seat region. The results obtained were fairly inaccurate.

A second important factor is the number of strain readings that are required to represent a particular loading (i.e., for accuracy and convergence). This is a difficult question as this depends upon the behavior of the applied loading function, which is as yet undetermined. Nevertheless a reasonable guess can be made from the experiments conducted. For a quadratic function, only five strain gauge readings were required to obtain a decent representation. But for convergence and high accuracy, approximately eight were required. Similarly for higher-order loads, eight strains were required. Again, for convergence and higher accuracy, 12 strain readings were required to represent the loading function. Thus, the numerical experimentation has indicated that the number and location of the strain measurements is critical to load recovery. Future research is required to determine an optimal approach with which maximum information can be derived from the experimental data.

Future Work

Additional tests are being conducted with the number and location of the strain gauges being specified based on the study reported herein. Future work in this area will include shear traction loads at these locations. The code ANTWIL can be readily modified and can be used for determining the shear traction loads. Finally, the results of this research should be coupled with methods to assess the durability and damage tolerance of the wheel.

Appendix

For an axisymmetric body with a general, even loading, the displacements can be written as a Fourier series in the θ direction as

$$\begin{Bmatrix} u \\ v \\ w \end{Bmatrix} = \sum_n \begin{bmatrix} u_n \cos(n\theta) \\ v_n \sin(n\theta) \\ w_n \cos(n\theta) \end{bmatrix} \tag{A1}$$

where u_n, v_n, and w_n are displacement amplitudes for the nth harmonic. The strain-displacement relation in cylindrical coordinates are given as

$$\begin{aligned} \epsilon_r &= \frac{\partial u}{\partial r} \\ \epsilon_\theta &= \frac{u}{r} + \frac{1}{r}\frac{\partial v}{\partial \theta} \\ \epsilon_z &= \frac{\partial w}{\partial z} \\ \gamma_{rz} &= \frac{\partial u}{\partial z} + \frac{\partial w}{\partial r} \\ \gamma_{r\theta} &= \frac{1}{r}\frac{\partial u}{\partial \theta} + \frac{\partial v}{\partial r} - \frac{v}{r} \\ \gamma_{\theta z} &= \frac{\partial v}{\partial z} + \frac{1}{r}\frac{\partial w}{\partial \theta} \end{aligned} \tag{A2}$$

Substituting Eq. (A1) into Eq. (A2) yields the Fourier series representation of the strains as

$$\begin{aligned} \epsilon_r &= \sum_n \frac{\partial u_n}{\partial r}\cos(n\theta) \equiv \sum_n \epsilon^c_{rn}\cos(n\theta) \\ \epsilon_\theta &= \sum_n [u_n + nv_n]\frac{\cos(n\theta)}{r} \equiv \sum_n \epsilon^c_{\theta n}\cos(n\theta) \\ \epsilon_z &= \sum_n \frac{\partial w_n}{\partial z}\cos(n\theta) \equiv \sum_n \epsilon^c_{zn}\cos(n\theta) \\ \gamma_{rz} &= \sum_n \left[\frac{\partial u_n}{\partial z} + \frac{\partial w_n}{\partial r}\right]\cos(n\theta) \equiv \sum_n \gamma^c_{rzn}\cos(n\theta) \\ \gamma_{r\theta} &= \sum_n \left[-\frac{n}{r}u_n + \frac{\partial v_n}{\partial r} - \frac{v_n}{r}\right]\sin(n\theta) \equiv \sum_n \gamma^s_{r\theta n}\sin(n\theta) \\ \gamma_{\theta z} &= \sum_n \left[\frac{\partial v_n}{\partial z} - \frac{n}{r}w_n\right]\sin(n\theta) \equiv \sum_n \gamma^s_{\theta zn}\sin(n\theta) \end{aligned} \tag{A3}$$

Thus, for the displacement representation given by Eq. (A1), ϵ_r, ϵ_θ, ϵ_z, and γ_{zr} are given by Fourier cosine series while $\gamma_{z\theta}$ and $\gamma_{\theta z}$ are given by Fourier sine series. The development above yields the Fourier series representation of the strains due to cosine series part of the loading. A similar procedure is used for the sine series part of the loading. The matrix or tensor representation of the strains then yield Eqs. (6) and (7).

Acknowledgment

We would like to thank the Landing Gear Systems Group, Flight Dynamics Laboratory at Wright-Patterson Air Force Base in Dayton, Ohio for their support of this project.

References

[1]Durap, P. C., and Brussat, T. R., "Wheel Performance Evaluation," FAA Technical Center, Atlantic City, NJ, June 1985.

[2]Treanor, D. H., and Boike, M. R., "Military Aircraft Wheel Load Spectrum Development," Flight Dynamics Lab., Wright Research and Development Center, WRDC-TR-3109, Wright-Patterson AFB, OH, Dec. 1988.

[3]Lawler, W. T., Spencer, B. F., Jr., and Enneking, T. J., "Damage Tolerance of Aircraft Wheel," Flight Dynamics Lab., Wright Research and Development Center, WRDC-TR-3109, Wright-Patterson AFB, OH, 1989.

[4]Mayer, A. H., "Fast Propagation of a Griffith Crack in Brittle Material and the Existence of Limiting Crack Speeds," Flight Dynamics Lab., Wright Research and Development Center, TM WRDC/FIV 90, Wright-Patterson AFB, OH, Dec. 1988.

[5]Ulrich, P., personal communication, Landing Gear Systems Group, Flight Dynamics Directorate, Wright-Patterson AFB, OH, Jan. 1991.

[6]Wagner, P. M., "Laboratory Evaluation of the Michelin 25.5 × 8.0 R 14/18 Ply Rating Aircraft Radial Tire," Flight Dynamics Lab., Wright Research and Development Center, Wright-Patterson AFB, OH, Aug. 1988.